NANO LETTERS

Letter

pubs.acs.org/NanoLett

Tuning the Electronic and Chemical Properties of Monolayer MoS_2 Adsorbed on Transition Metal Substrates

Wei Chen,[†,‡,§] Elton J. G. Santos,[*,§] Wenguang Zhu,[*,‡,†] Efthimios Kaxiras,[§] and Zhenyu Zhang[‡,§]

[†]Department of Physics and Astronomy, University of Tennessee, Knoxville, Tennessee 37996, United States

[‡]ICQD, Hefei National Laboratory for Physical Sciences at the Microscale, University of Science and Technology of China, Hefei, Anhui 230026, China

[§]Department of Physics and School of Engineering and Applied Sciences, Harvard University, Cambridge, Massachusetts 02138, United States

ABSTRACT: Using first-principles calculations within density functional theory, we investigate the electronic and chemical properties of a single-layer MoS_2 adsorbed on Ir(111), Pd(111), or Ru(0001), three representative transition metal substrates having varying work functions but each with minimal lattice mismatch with the MoS_2 overlayer. We find that, for each of the metal substrates, the contact nature is of Schottky-barrier type, and the dependence of the barrier height on the work function exhibits a partial Fermi-level pinning picture. Using hydrogen adsorption as a testing example, we further demonstrate that the introduction of a metal substrate can substantially alter the chemical reactivity of the adsorbed MoS_2 layer. The enhanced binding of hydrogen, by as much as ~0.4 eV, is attributed in part to a stronger H−S coupling enabled by the transferred charge from the substrate to the MoS_2 overlayer, and in part to a stronger MoS_2-metal interface by the hydrogen adsorption. These findings may prove to be instrumental in future design of MoS_2-based electronics, as well as in exploring novel catalysts for hydrogen production and related chemical processes.

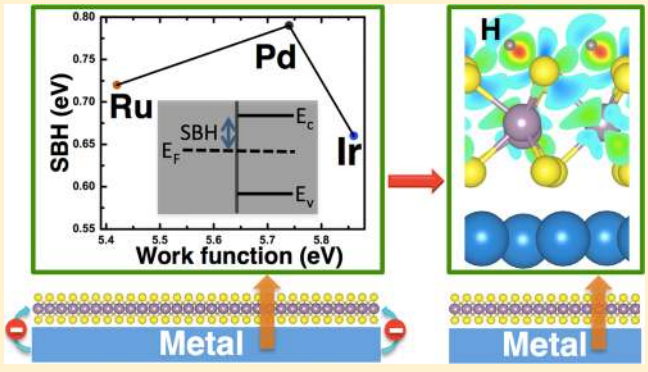

KEYWORDS: *Density functional theory, MoS_2-metal contacts, Schottky barrier, hydrogen adsorption, catalyst*

As a transition-metal dichalcogenide semiconductor, MoS_2 is a commonly used dry lubricant, whose low-dimensional structures are receiving much research attention because of their distinctive electronic,[1−3] optical,[1,4−6] and catalytic properties.[7−11] Bulk MoS_2 has a layered structure, each layer consisting of a covalently bonded S−Mo−S hexagonal quasi-two-dimensional network,[12,13] with weak van der Waals (vdW) attraction between the layers. Owing to the relatively weak interlayer interaction, a monolayer of MoS_2 can be mechanically exfoliated from a MoS_2 crystal.[14] Such monolayer systems not only have a direct band gap with highly desirable optical properties[1] but also possess sufficiently high carrier mobility for potential applications in nanoelectronics.[15] In exploring the device potential of monolayer MoS_2, it is vital to understand how such systems interface with metallic contacts, similar to recent developments in other areas of nanomaterials such as semiconductor wires, carbon nanotubes,[16,17] and graphene.[18] In particular, it was found recently that both the barrier height for electron tunneling and the nature of contact between MoS_2 and an electrode can be drastically altered when using different types of metal contacts.[19] Furthermore, on a different front, monolayer-high MoS_2 islands adsorbed on different metal substrates have been shown to be highly catalytic in hydrogen evolution reaction (HER),[8−11] with the reactivity largely attributed to the edge sites of the islands.

In this Letter, we use first-principles calculations within density functional theory (DFT) to investigate the electronic and chemical properties of a single-layer MoS_2 adsorbed on Ir(111), Pd(111), or Ru(0001), three representative transition metal substrates having varying work functions but each with minimal lattice mismatch with the MoS_2 overlayer. We find that for each of the metal substrates, the contact nature is of Schottky-barrier type, and the dependence of the barrier height on the work function establishes a partial Fermi-level (FL) pinning picture.[20] Using hydrogen adsorption as a testing example, we further demonstrate that the introduction of a metal substrate can substantially alter the chemical reactivity of the adsorbed MoS_2 layer. Our detailed analysis of the electron density redistribution reveals that the enhanced binding of hydrogen, by as much as ~0.4 eV, is attributed in part to a stronger H−S coupling enabled by the transferred charge from the substrate to the MoS_2 overlayer, and in part to a stronger MoS_2-metal interface by the hydrogen adsorption. These

Received: October 24, 2012
Revised: January 8, 2013
Published: January 15, 2013

findings may prove to be instrumental in future design of MoS_2-based electronics, as well as in exploring novel catalysts for hydrogen production and related chemical processes.

Our DFT calculations were carried out using the Vienna *ab initio* simulation package (VASP)[21] with projector-augmented wave (PAW) pseudopotentials[22,23] and the Ceperley-Alder local density approximation (LDA)[24] as parametrized by Perdew and Zunger[25] for the exchange-correlation functional. Unless otherwise specified, the results presented were from LDA calculations. For Pd and Ru as substrates, we have also compared the LDA results with those from DFT-D2,[26,27] a semiempirical approach that includes vdW interactions, to cross check on the accuracy as well as the overall trends of the LDA results.[28] The lattice constants of the metals and the monolayer MoS_2 were obtained via structural optimization. The metal substrates were modeled by slabs of 8 atomic layers, and the MoS_2-metal systems were modeled by placing a single-layer MoS_2 on top of the metal surfaces. A vacuum region more than 15 Å was used to ensure decoupling between neighboring slabs. During structural relaxation, only the bottom layer atoms were fixed in their respective bulk positions, with all the other atoms fully relaxed until the force on any given atom is smaller than 0.01 eV/Å. A $6 \times 6 \times 1$ *k*-point mesh was used for the 2×2 surface unit cell of metals.[29] When H adsorption was considered, we also examined the effect of spin polarization in our calculations. The spin−orbit coupling effect has also been checked for the heaviest element, Ir, and the detailed results indicate that it has only negligible influence on the energetics.

We choose Ir(111), Pd(111), and Ru(0001) as substrates mainly because a $(\sqrt{3} \times \sqrt{3})$ R30° unit cell of MoS_2 can nicely match with a 2×2 unit cell of Ir(111), Pd(111), or Ru(0001), as illustrated in Figure 1. The maximum mismatch is ~1.2% for

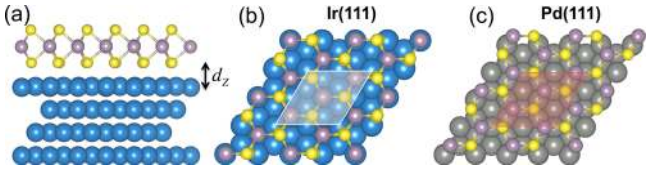

Figure 1. (a) Side and (b) top views of monolayer MoS_2 on the Ir(111) substrate. (c) Top view of MoS_2 on the Pd(111) substrate. In b and c, the white- and red-shaded areas show the unit cells in the calculations, respectively.

Ru(0001), with varying work functions of 5.86 eV, 5.74 eV, and 5.42 eV for Ir(111), Pd(111), and Ru(0001), respectively. In our calculations, the surface lattices of the metal substrates were fixed to their optimized values and the in-plane lattice of MoS_2 was adjusted to match the metal substrates accordingly. The most stable contact geometries were obtained by optimizing the structures from different initial configurations. For all of the systems, the top layer of the metal substrates and the bottom S layer of MoS_2 essentially stay planar after relaxation, with the MoS_2-metal distances listed in Table 1. However, the relative positions between MoS_2 and the substrates along the interface directions are different for different metals. On Ir(111), the three Mo atoms in the supercell sit above the fcc hollow, hcp hollow, and top sites, respectively (Figure 1b); while on Pd(111), the Mo atoms are all above the centers of the triangles formed by the fcc, hcp, and top sites (Figure 1c). The registry of MoS_2 relative to the top layer of Ru(0001) is similar to that of Ir(111) and is therefore omitted in Figure 1. The MoS_2-

Table 1. Structural and Energetic Results for All of the Free-Standing MoS_2 and MoS_2-Metal Systems[a]

	E_b (eV)	d_z^0 (Å)	d_z^H (Å)	E_a (eV)	L_{H-S} (Å)	θ (deg)
free-standing MoS_2				1.07	1.46	40.2
MoS_2/Ir(111)	0.62	2.23	2.20	1.44	1.43	37.2
MoS_2/Pd(111)	0.74	2.17	2.09	1.39	1.39	89.1
MoS_2/Ru(0001)	0.82	2.25	2.20	1.33	1.46	38.2

[a] E_b is the binding energy per sulfur atom between MoS_2 and a given substrate; d_z^0 and d_z^H are the distances between MoS_2 and a given metal substrate without and with H adsorption, respectively; E_a is the H binding energy on the planar surface of a free-standing MoS_2 or a MoS_2 overlayer on a given substrate; L_{H-S} is the H−S bond length; θ is the angle between the H−S bond and the planar surface of MoS_2.

metal binding energies per interfacial sulfur atom, calculated as $E_b = (E_{MoS_2} + E_{metal} - E_{MoS_2/metal})/3$, range from 0.62 to 0.82 eV as listed in Table 1. The inclusion of the vdW interactions increases the binding energy by 0.16 eV for Pd and 0.19 eV for Ru; furthermore, the GGA-vdW results also reduce the interfacial distances between the MoS_2 overlayer and the metal substrates to be close to the LDA results. The even stronger binding energies of the vdW results over LDA, which tends to overestimate the binding,[30] should be attributed to the significant attractive contributions of vdW interactions.

To identify the energy level alignment at the interface between MoS_2 and the metal substrates, we have calculated the band structures of MoS_2 and the combined systems. As seen in Figure 2a, the original K point of the 1×1 unit cell where the band edge is located, is folded to the Γ point in the reciprocal space of the $\sqrt{3} \times \sqrt{3}$ superlattice of single-layer MoS_2. The calculated band gap is ~1.8 eV, consistent with previous results.[1,2] In the combined systems, although the energy bands of MoS_2 hybridize with those of the metals to a certain extent, the majority of the MoS_2 bands can still be identified, as marked in red in Figure 2b−d. The FLs of the combined systems always lie in the band gap region of MoS_2, resulting in the formation of a Schottky barrier at the interface for each case. The calculated n-type Schottky barrier heights corresponding to the energy differences between the conduction band minimum and the FLs are 0.66 eV, 0.79 eV, and 0.72 eV for Ir, Pd, and Ru, respectively (Figure 2e). The maximal work function difference is 0.44 eV, while the maximal difference in the Schottky barrier heights is 0.13 eV; we therefore observe a *partial* FL pinning picture[20] when the three metals form contacts with monolayer MoS_2. As for likely pinning mechanisms, the picture of metal-induced gap states is typically operative deep in the semiconductor,[31] suggesting that a single layer of MoS_2 is unlikely to cause strong FL pinning, consistent with the present study. Alternatively, we expect that the sufficiently strong chemical bonding at the interface, the other pinning mechanism,[32] may have also contributed to the pinning effects.

There is another angle to view the electronic properties and contact nature at the MoS_2-metal interfaces. If the FL pinning effects were absent, we would have expected Schottky barrier heights of roughly 1.5 eV, 1.4 eV, and 1.1 eV for Ir, Pd, and Ru, respectively, given by the separations between the conduction band minimum and the FL of the monolayer MoS_2 subtracted by the respective work function differences of MoS_2 and Ir, Pd, or Ru. The observed Schottky barrier heights indicate that there exist pronounced FL shifts of the adsorbed MoS_2, given by ~1.11 eV, 0.98 eV, and 1.05 eV for Ir, Pd, and Ru, respectively.

dx.doi.org/10.1021/nl303909f | *Nano Lett.* 2013, 13, 509−514

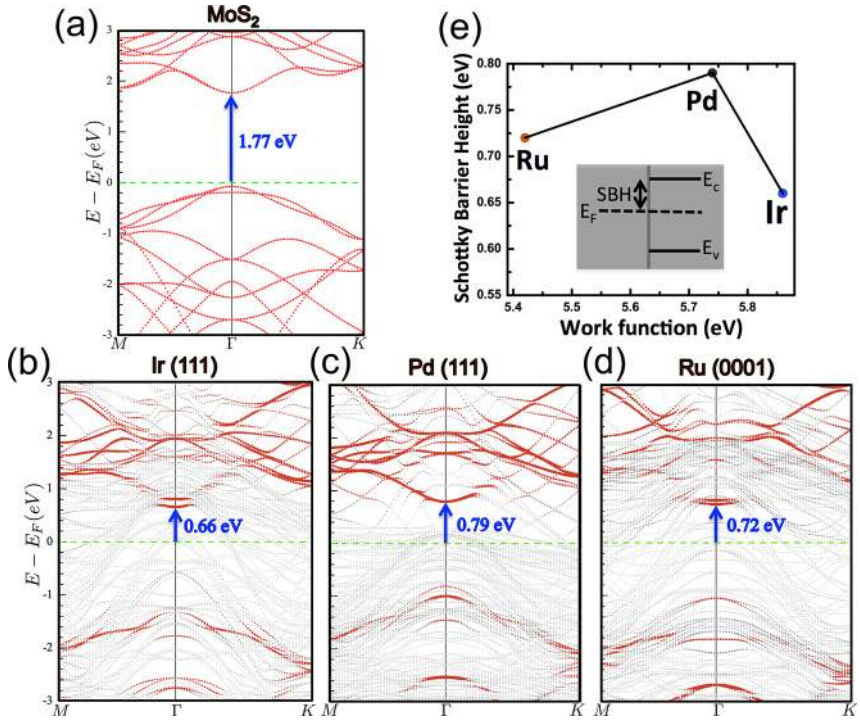

Figure 2. Band structures of (a) a $\sqrt{3} \times \sqrt{3}$ superlattice of monolayer MoS_2, (b) MoS_2–Ir(111), (c) MoS_2–Pd(111), and (d) MoS_2–Ru(0001) interfaces. The Fermi energy E_F is set to zero in all of the four panels and is indicated by the green dashed lines. In b–d, the red lines correspond to the energy bands of the monolayer MoS_2, and the numbers in blue are the Schottky barrier heights, whose dependence on the work function of the metal substrate is plotted in e.

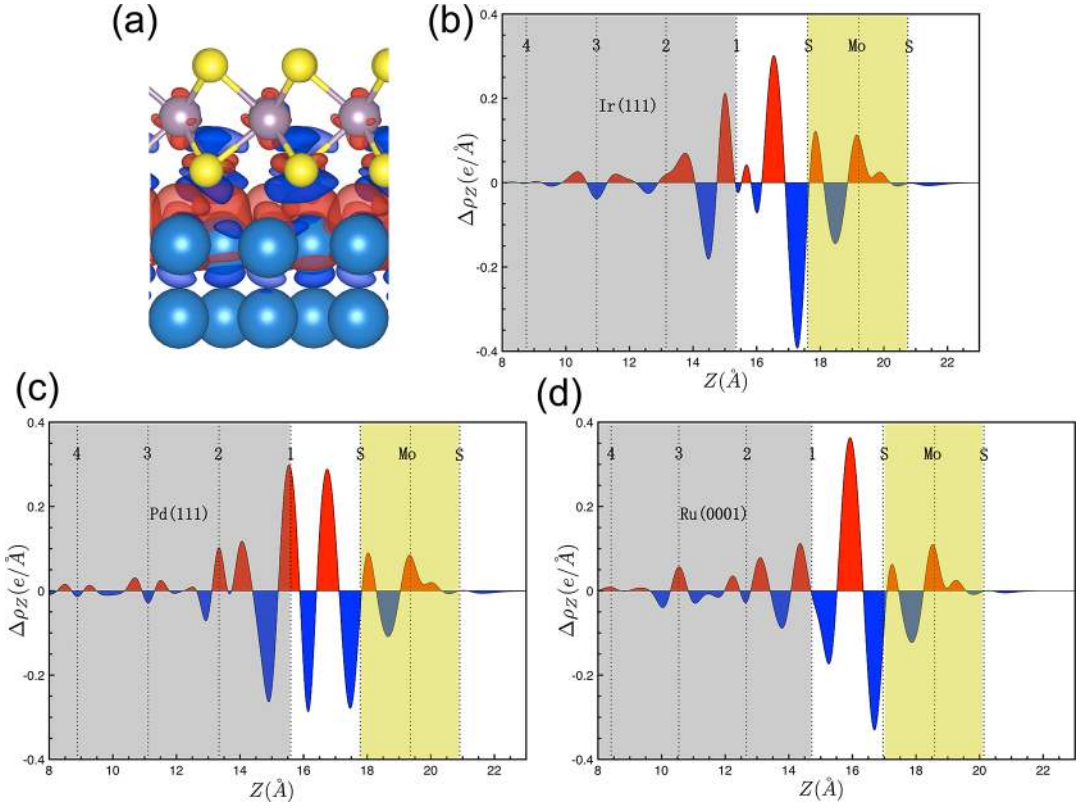

Figure 3. (a) Side view of the charge difference between the combined MoS_2–Ir(111) system and the sum of the isolated MoS_2 and Ir substrate. (b–d) Plots of the plane-averaged electron density difference along the direction perpendicular to the interface ($\Delta\rho_z$) of MoS_2–Ir(111) (b), MoS_2–Pd(111) (c), and MoS_2–Ru(0001) (d). For each case, the reference location Z = 0 Å is taken to be the position of the bottom layer of the metal substrate in the slab. The red and blue colors indicate electron accumulation and depletion, respectively.

dx.doi.org/10.1021/nl303909f | Nano Lett. 2013, 13, 509–514

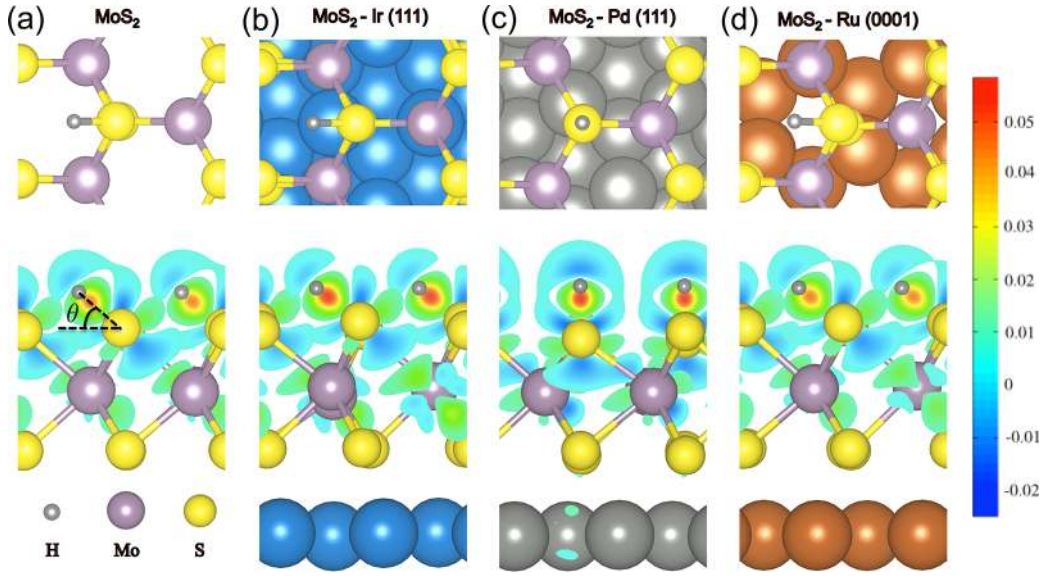

Figure 4. Top views of the bonding geometries (upper row) and cross-sectional views of the charge transfer density (lower row) between a H atom and (a) a free-standing MoS_2, (b) the MoS_2/Ir(111), (c) MoS_2/Pd(111), and (d) MoS_2/Ru(0001) systems. The red and blue colors represent the maximum charge accumulation and maximum charge depletion, respectively.

Similarly, additional FL shifts of up to ~0.5 eV were also observed in a previous study of graphene–metal contacts.[33,34] In both cases, such FL shifts can be induced by the resultant effects of charge transfer at the interfaces and chemical bonding effects; the larger and nonlinear FL shifts are also consistent with the much stronger and varying chemical bondings in the present systems.

To further illustrate the detailed nature of the charge transfer at the MoS_2-metal interfaces, we show in Figure 3a the charge difference between the combined MoS_2–Ir(111) system and the sum of the isolated MoS_2 and Ir substrate. The electronic structures of the isolated MoS_2 and Ir substrate were calculated by freezing the atomic positions of the respective components as obtained in the combined system. The red regions represent accumulation, and the blue regions represent depletion of electrons in the combined system relative to the two isolated components. To have a quantitative picture, we plot in Figure 3b–d the plane-averaged electron density difference $\Delta\rho_z$ along the perpendicular direction to the interface. Several charge transfer oscillations are observed at the interfacial region, and some extra charge is found to accumulate around the Mo atoms. Since the position of MoS_2 on Pd(111) is different from that on Ir(111) or Ru(0001), there is a net charge accumulation in the first layer of the Pd substrate closest to MoS_2 (Figure 3c), while the first layer of the Ir and Ru substrates is located at places where the net charge transfer is negligible (Figure 3b and d). Overall, the oscillatory nature of the charge transfer at the interfaces is complex, but our analysis on the FL shifts given above indicates that the adsorbed MoS_2 is net n-type doped by the three investigated metals.

Aside from the transport properties for potential electronic device applications, the significant charge transfer at the MoS_2-metal contacts is also expected to affect the chemical properties of the MoS_2 overlayer. To explore the possibility of tuning the chemical reactivity on the planar surface of MoS_2 through metal substrates, we consider HER as a testing case, which is fundamentally important in a variety of electrochemical processes of technological significance. Currently the most efficient HER catalyst is Pt, which is a precious metal, making it highly desirable to find alternative catalysts based on materials that are abundant and of low cost. MoS_2 has been demonstrated the ability to function as a HER catalyst, but only the edge sites of the monolayer MoS_2 clusters were identified to be chemically reactive while the planar surface is rather inert.[10] Due to the small lattice mismatches between MoS_2 and the metal substrates considered here, it is expected that large-scale monolayer MoS_2 sheets can be grown on these substrates. Although the planar surface of MoS_2 cannot be as catalytic as the edge sites, considering the large area of the planar surfaces, it is appealing to gain stronger overall reactivity by making the whole planar surfaces sufficiently catalytic. A critical step in HER is that a H^+ ion gains an electron from the electrode, becoming an atomic H, whose binding energy on the catalytic MoS_2 overlayer placed on the electrode is yet another vital energy scale determining the overall HER efficiency. For this important reason and also for simplicity, we study the influence of different metal substrates on the adsorption energy of atomic H on the MoS_2 overlayer, leaving the electron capture process of H^+ for a future study.

To find the most stable adsorption site of H on the surface of a given MoS_2 overlayer, we have examined all possible initial positions based on symmetry considerations. Figure 4 depicts the top and side views of the most stable H adsorption geometries on the three metal substrates. The corresponding adsorption energies, calculated as $E_a = E_{hydrogen} + E_{substrate} - E_{hydrogen/substrate}$, are 1.44 eV, 1.39 eV, and 1.33 eV for Ir, Pd, and Ru, respectively (Table 1), all of which are substantially enhanced from the value of 1.07 eV on a free-standing MoS_2. We have verified that the DFT-D2 calculations yield only slightly enhanced binding energies over the LDA results (by less than 0.02 eV). In addition to the binding energy differences, we also observe geometrical differences between the considered systems, as measured by θ, the angle between the H–S bond and the planar surface of MoS_2. As shown in Figure 4 and Table 1, for the systems of MoS_2–Ir(111) and MoS_2–Ru(0001), θ is 37.2° and 38.2°, similar to the angle of 40.2° on the free-standing MoS_2. In contrast, the H adatom prefers an atop position on MoS_2–Pd(111), with $\theta \approx 90°$,

dx.doi.org/10.1021/nl303909f | Nano Lett. 2013, 13, 509–514

caused by the dramatically different atomic registry between the MoS_2 overlayer and the first layer of the Pd substrate when compared with the other two substrates. Collectively, these results show that both the H binding energy and binding geometry can be tuned with a proper choice of the metal electrode; such tunabilities, in turn, can significantly affect the HER efficiency of the planar MoS_2 overlayer.

To reveal the physical origin of the substrate-enhanced H binding energy, we have calculated the charge transfer between H and the surfaces measured by $\Delta\rho = \rho_{H/MoS_2/metal} - \rho_H - \rho_{MoS_2/metal}$. The panels shown in the lower row of Figure 4 display the side views of the contour plots of $\Delta\rho$, taken in the plane normal to the interface and across the H−S bond. We see a clear indication that more charge is involved in the covalent H−S bonds on the Ir(111) and Pd(111) substrates, which is also consistent with the shortened bond lengths shown in Table 1. In contrast, little change is observed in the H−S bond on Ru(0001) from the free-standing MoS_2 case, consistent with the observation that the enhancement in the adsorption energy is the smallest among the three metals. Aside from the charge redistribution between the H adatom and the MoS_2 overlayer, we can also investigate the effect of H adsorption on the coupling between the MoS_2 and the substrate. Such effects could be quantified by variations in d_z^H, defining the maximum separation of the sulfur atoms in the lower layer of MoS_2 from the topmost layer of the metal substrate. When compared with d_z^0, the separation without the presence of H, d_z^H becomes smaller by 0.03 Å, 0.08 Å, and 0.05 Å for Ir, Pd, and Ru, respectively. These results demonstrate that the enhancements in the adsorption energy arise from two aspects: one is the stronger H−S covalent bonding enabled by the transferred charge from the metal substrates to MoS_2; the other is associated with the stronger MoS_2-metal interfaces caused by the H adatom serving as a "nail" to pin the MoS_2 and substrate together.

Before closing, we note that the significant net charge transfer from the metal substrates to the MoS_2 overlayer will likely have an even stronger effect on the electron capture process of H^+ ion. This intriguing possibility will be examined in a future study of a more complete HER cycle.

In summary, we have investigated the electronic and chemical properties of a single-layer MoS_2 adsorbed on Ir(111), Pd(111), or Ru(0001). We found that for each of the metal substrates, the contact nature is of Schottky-barrier type, and the dependence of the Schottky barrier height on the work function establishes a partial Fermi-level pinning picture for these systems. We have further demonstrated that the introduction of a metal substrate can substantially alter the H binding energy on the MoS_2 overlayer. A detailed analysis of the electron density redistribution revealed that the enhanced binding of hydrogen is the result of a stronger H−S coupling enabled by the transferred charge from the substrate to the MoS_2 overlayer, and a stronger MoS_2-metal interaction caused by the hydrogen adsorption. These findings may prove to be instrumental in future design of MoS_2-based electronics, as well as in searching for novel catalysts for hydrogen production and related chemical processes.

AUTHOR INFORMATION

Corresponding Author

*E-mails: esantos@seas.harvard.edu (E.J.G.S.) and wgzhu@ustc.edu.cn (W.Z.)

Notes

The authors declare no competing financial interest.

ACKNOWLEDGMENTS

This work was supported by the U.S. National Science Foundation (W.C. and Z.Z., Grant No. 0906025), National Natural Science Foundation of China (Grant No. 11034006), and the U.S. Department of Energy (W.Z. and Z.Z., Grant No. DE-FG03-02ER45958). This research used resources of the National Energy Research Scientific Computing Center, which is supported by the Office of Science of the U.S. Department of Energy under Contract No. DE-AC02-05CH11231.

REFERENCES

(1) Mak, K. F.; Lee, C.; Hone, J.; Shan, J.; Heinz, T. F. *Phys. Rev. Lett.* **2010**, *105*, 136805.
(2) Han, S. W.; Kwon, H.; Kim, S. K.; Ryu, S.; Yun, W. S.; Kim, D. H.; Hwang, J. H.; Kang, J.-S.; Baik, J.; Shin, H. J.; Hong, S. C. *Phys. Rev. B* **2011**, *84*, 045409.
(3) Li, Y.; Zhou, Z.; Zhang, S. B.; Chen, Z. F. *J. Am. Chem. Soc.* **2008**, *130*, 16739.
(4) Splendiani, A.; Sun, L.; Zhang, Y. B.; Li, T.; Kim, J.; Chim, C.; Galli, G.; Wang, F. *Nano Lett.* **2010**, *10*, 1271.
(5) Zeng, H.; Dai, J.; Yao, W.; Xiao, D.; Cui, X. *Nat. Nanotechnol.* **2012**, *7*, 490.
(6) Mak, K. F.; He, K.; Shan, J.; Heinz, T. F. *Nat. Nanotechnol.* **2012**, *7*, 494.
(7) Moses, P. G.; Hinnemann, B.; Topsøe, H.; Nørskov, J. K. *J. Catal.* **2007**, *248*, 188.
(8) Hinnemann, B.; Moses, P. G.; Bonde, J.; Jørgensen, K. P.; Nielsen, J. H.; Horch, S.; Chorkendorff, I.; Nøskov, J. K. *J. Am. Chem. Soc.* **2005**, *127*, 5308.
(9) Bonde, J.; Moses, P. G.; Jaramillo, T. F.; Nøskov, J. K.; Chorkendorff, I. *Faraday Discuss.* **2008**, *140*, 219.
(10) Jaramillo, T. F.; Jørgensen, K. P.; Bonde, J.; Nielsen, J. H.; Horch, S.; Chorkendorff, I. *Science* **2007**, *317*, 100.
(11) Li, Y.; Wang, H.; Xie, L.; Liang, Y.; Hong, G.; Dai, H. *J. Am. Chem. Soc.* **2011**, *133*, 7296.
(12) Helveg, S.; Lauritsen, J. V.; Lægsgaard, E.; Stensgaard, I.; Nøskov, J. K.; Clausen, B. S.; Topsøe, H.; Besenbacher, F. *Phys. Rev. Lett.* **2000**, *84*, 951.
(13) Lauritsen, J. V.; Kibsgaard, J.; Helveg, S.; Topsøe, H.; Clausen, B. S.; Lægsgaard, E.; Besenbacher, F. *Nat. Nanotechnol.* **2007**, *2*, 53.
(14) Novoselov, K. S.; Jiang, D.; Schedin, F.; Booth, T. J.; Khotkevich, V. V.; Morozov, S. V.; Geim, A. K. *Proc. Natl. Acad. Sci. U.S.A.* **2005**, *102*, 10451.
(15) Radisavljevic, B.; Radenovic, A.; Brivio, J.; Giacometti, V.; Kis, A. *Nat. Nanotechnol.* **2011**, *6*, 147.
(16) Zhu, W. G.; Kaxiras, E. *Nano Lett.* **2006**, *6*, 1415.
(17) Zhu, W. G.; Kaxiras, E. *Appl. Phys. Lett.* **2006**, *89*, 243107.
(18) Léonard, F.; Talin, A. A. *Nat. Nanotechnol.* **2011**, *6*, 773.
(19) Popov, I.; Seifert, G.; Tománek, D. *Phys. Rev. Lett.* **2012**, *108*, 156802.
(20) Kurtin, S.; McGill, T. C.; Mead, C. A. *Phys. Rev. Lett.* **1969**, *22*, 1433.
(21) Kresse, G.; Furthmüller, J. *Phys. Rev. B* **1996**, *54*, 11169.
(22) Blöchl, P. E. *Phys. Rev. B* **1994**, *50*, 17953.
(23) Kresse, G.; Joubert, D. *Phys. Rev. B* **1999**, *59*, 1758.
(24) Ceperley, D. M.; Alder, B. J. *Phys. Rev. Lett.* **1980**, *45*, 566.
(25) Perdew, J. P.; Zunger, A. *Phys. Rev. B* **1981**, *23*, 5048.
(26) Grimme, S. *J. Comput. Chem.* **2006**, *27*, 1787.
(27) Bučko, T.; Hafner, J.; Lebègue, S.; Ángyán, J. G. *J. Phys. Chem. A* **2010**, *114*, 11814.
(28) Schimka, L.; Harl, J.; Stroppa, A.; Grüneis, A.; Marsman, M.; Mittendorfer, F.; Kresse, G. *Nat. Mater.* **2010**, *9*, 741.
(29) Methfessel, M.; Paxton, A. T. *Phys. Rev. B* **1989**, *40*, 3616.
(30) Gao, Y.; Zeng, X. C. *J. Phys.: Condens. Matter* **2007**, *19*, 386220.

(31) Tersoff, J. *Phys. Rev. Lett.* **1984**, *52*, 465.
(32) Tung, R. T. *Phys. Rev. Lett.* **2000**, *84*, 6078.
(33) Giovannetti, G.; Khomyakov, P. A.; Brocks, G.; Karpan, V. M.; van den Brink, J.; Kelly, P. J. *Phys. Rev. Lett.* **2008**, *101*, 026803.
(34) Khomyakov, P. A.; Giovannetti, G.; Rusu, P. C.; Brocks, G.; van den Brink, J.; Kelly, P. J. *Phys. Rev. B* **2009**, *79*, 195425.